Direct numerical simulation of a plane turbulent wall-jet including scalar mixing

Daniel Ahlman, Geert Brethouwer, and Arne V. Johansson
Linné Flow Centre, Department of Mechanics, Royal Institute of Technology, SE-100 44 Stockholm, Sweden

(Received 10 July 2006; accepted 13 March 2007; published online 7 June 2007)

Direct numerical simulation is used to study a turbulent plane wall-jet including the mixing of a passive scalar. The Reynolds and Mach numbers at the inlet are Re=2000 and $M=0.5$, respectively, and a constant coflow of 10% of the inlet jet velocity is used. The passive scalar is added at the inlet enabling an investigation of the wall-jet mixing. The self-similarity of the inner and outer shear layers is studied by applying inner and outer scaling. The characteristics of the wall-jet are compared to what is reported for other canonical shear flows. In the inner part, the wall-jet is found to closely resemble a zero pressure gradient boundary layer, and the outer layer is found to resemble a free plane jet. The downstream growth rate of the scalar is approximately equal to that of the streamwise velocity in terms of the growth rate of the half-widths. The scalar fluxes in the streamwise and wall-normal direction are found to be of comparable magnitude. The scalar mixing situation is further studied by evaluating the scalar dissipation rate and the mechanical to mixing time scale ratio. © *2007 American Institute of Physics*. [DOI: 10.1063/1.2732460]

I. INTRODUCTION

A plane wall-jet is obtained by injecting fluid parallel to a wall in such a way that the velocity of the fluid, over some distance from the wall, supersedes that of the ambient flow. The structure of a turbulent wall-jet can be described as being composed of two canonical shear layers of different type. The inner shear layer, reaching from the wall out to the point of maximum streamwise velocity, resembles a boundary layer, while the outer layer, from the maximum velocity out to the ambient fluid, resembles a free shear layer. A consequence of the double shear layer structure is that properties such as momentum transfer and mixing will exhibit distinctively different characteristics and scaling properties in the two shear layers.

Plane wall-jets are used in a wide range of engineering applications. Many of these applications apply wall-jets to modify heat and mass transfer close to walls. Well known examples of these are, e.g., film-cooling of the leading edges of turbine blades and in automobile demisters. In these applications, turbulent mixing in the vicinity of walls plays an important role. However, the mixing processes in this region are presently not fully understood, and it is therefore of interest to add to this knowledge.

The first experimental work on turbulent plane wall-jets was carried out by Förthmann.[1] The investigation concluded that the mean velocity field develops in a self-similar manner, that the half-width grows linearly, and that the maximum velocity is inversely proportional to the square root of the downstream distance. Glauert[2] studied the wall-jet theoretically, seeking a similarity solution to the mean flow by applying an empirical eddy viscosity model. However, because different eddy viscosities are needed in the inner and outer part of the jet, he concluded that a single similarity solution is not possible. Bradshaw and Gee[3] were the first to present turbulence measurements from a wall-jet and reported that the shear stress attains a finite value at the point of maximum velocity. Tailland and Mathieu[4] reported a Reynolds number dependency of the half-width growth and maximum velocity decay.

The wall-jet experiments carried out prior to 1980 have been compiled and critically reviewed by Launder and Rodi.[5,6] In the experiments considered to be satisfactorily two-dimensional, the linear spreading rates were found to fall within the range $dy_{1/2}/dx=0.073\pm0.002$. The position of zero shear stress was also concluded to be displaced from the position of maximum velocity, but the uncertainties in the turbulence statistics were reported to be high. In the experiments reviewed, no near-wall peak in the energy was found, which was assumed to result from a strong influence of the free shear layer on the inner layer. In the experimental study of Abrahamsson *et al.*,[7] inner maxima were found in the streamwise and lateral turbulence intensities but not in the turbulent kinetic energy profile.

Schneider and Goldstein[8] used laser Doppler velocimetry (LDV) to measure turbulence statistics in a wall-jet at Re=14000. They found the Reynolds stresses in the outer region to be higher than in previous experiments using hot-wire measurements, which in turn were argued to underestimate properties in this region due to high turbulence intensities and flow reversals. LDV was also used by Eriksson *et al.*[9] to perform highly resolved velocity measurements in a wall-jet of Re=9600 all the way into the viscous sublayer, enabling direct determination of the wall shear stress.

Scaling laws for the mean profiles and the turbulence properties have previously been sought for the plane wall-jet. One choice is to use the inlet velocity and jet height as characteristic scales, but this scaling does not lead to collapse of data from experiments at different Reynolds numbers; see, e.g., Launder and Rodi.[5] Narashima *et al.*[10] suggested that the mean flow parameters should scale with the jet momen-

tum flux and the kinematic viscosity. The same approach was employed by Wygnanski *et al.*[11] in an effort to remove the inlet Reynolds number dependency and to determine the skin friction from the decrease in momentum flux. Irwin[12] used a momentum balance approach, neglecting viscous stresses, to derive that in the case of a jet in a coflow, the ratio of the streamwise velocity to the coflow must be kept constant to admit self-similarity. Zhou and Wygnanski[13] proposed a scaling based on the work of Narashima *et al.*[10] for the wall-jet in an external stream. George *et al.*[14] performed a similarity analysis of the inner and outer part of the wall-jet without coflow. Both the inner and shear layers were reported to reduce to similarity solutions of the boundary layer equations in the limit of infinite Reynolds number, but for finite Reynolds numbers, they found neither inner nor outer scaling to give a complete collapse of the data.

Dejoan and Leschziner[15] performed a large eddy simulation (LES) matching the experiments by Eriksson *et al.*[9] The results of the simulation agreed well with the experiments for the velocities and for the Reynolds stresses. An extensive study of the budgets of the turbulent energy and Reynolds stress was carried out, and turbulent transport was found to play a particularly important role in the region where the outer and inner layers overlap. The transition process in the experiments was reportedly difficult to accurately reproduce in the LES, and a discrepancy in the wall-normal stress in the simulation was attributed to this difficulty.

Reports of direct numerical simulations (DNS) of wall-jets have until recently been scarce. Wernz and Fasel[16,17] employed DNS to investigate instability mechanisms in a transitional wall-jet. The breakdown of a finite-aspect-ratio wall-jet was studied by Visbal *et al.*[18] Recently, Levin *et al.*[19] studied the laminar breakdown of a wall-jet using linear analysis and DNS. In an extension to that work, Levin[20] used a larger computational box to obtain averaged turbulence statistics.

Despite the numerous investigations of wall-jets, including theoretical, experimental, and numerical studies, the question of self-similarity and scaling has not been fully addressed. The reason for this originates in the existence of two different types of shear layers. Each of the layers have a distinct set of characteristics and scalings that excludes a full self-similarity. Presumably statistics close to the wall are governed by inner scales, in accordance with boundary layers, and likewise in the outer part, where some type of outer scales should be the appropriate ones. However, the definition of these scalings is not clear, and may as well vary between different quantities.

The aim of the present investigation is to study the turbulent propagation of a plane wall-jet by means of direct numerical simulation. The study aims at increasing the knowledge of the dynamics and mixing present in this flow case. The dynamics and self-similarity of the wall-jet is assessed by applying different scalings in the inner and outer shear layers. The mixing is analyzed through statistics of the passive scalar, the fluctuation, flux, and the dissipation rate. As for the dynamic properties, different scalings are employed to emphasize mixing properties in the inner and outer shear layer. Presently, few simulations have been performed for this flow case, and to our knowledge this is the first to include scalar mixing. The research performed is part of an ongoing project with the aim of studying turbulent combustion through DNS. The code used employs the fully compressible formulation in order to facilitate a later extension to reactive flows.

II. GOVERNING EQUATIONS

The equations governing conservation of mass, momentum, and energy used in the simulation are[21]

$$\frac{\partial \rho}{\partial t} + \frac{\partial \rho u_j}{\partial x_j} = 0, \tag{1}$$

$$\frac{\partial \rho u_i}{\partial t} + \frac{\partial \rho u_i u_j}{\partial x_j} = -\frac{\partial p}{\partial x_i} + \frac{\partial \tau_{ij}}{\partial x_j}, \tag{2}$$

$$\frac{\partial \rho E}{\partial t} + \frac{\partial \rho E u_j}{\partial x_j} = -\frac{\partial q_j}{\partial x_j} + \frac{\partial [u_i(\tau_{ij} - p\delta_{ij})]}{\partial x_j}, \tag{3}$$

where ρ is the mass density of the fluid, u_i is the velocity components, p is the pressure, and $E=(e+1/2u_iu_i)$ is the total energy. The fluid is considered to be Newtonian, with a zero bulk viscosity, for which the general form of the viscous stress is

$$\tau_{ij} = \mu\left(\frac{\partial u_i}{\partial x_j} + \frac{\partial u_j}{\partial x_i}\right) - \frac{2}{3}\mu\frac{\partial u_k}{\partial x_k}\delta_{ij}, \tag{4}$$

where μ is the dynamic viscosity. The heat diffusion is approximated using Fourier's law for the heat fluxes $q_i=-\lambda\partial T/\partial x_i$, where λ is the coefficient of thermal conductivity and T is the temperature. In the simulations, a Prandtl number of $\mathrm{Pr}=\mu c_p/\lambda=0.72$ is used. The fluid is furthermore assumed to be calorically perfect and to obey the perfect gas law. The mixing in the plane wall-jet is studied by introducing a passive scalar. The scalar is conserved and passive in the sense that the motion of the fluid is unaffected by the presence of the scalar. The equation governing the passive scalar concentration θ is[21]

$$\frac{\partial \rho\theta}{\partial t} + \frac{\partial}{\partial x_j}(\rho u_j\theta) = \frac{\partial}{\partial x_j}\left(\rho\mathcal{D}\frac{\partial\theta}{\partial x_j}\right), \tag{5}$$

where $\mathcal{D}$ is the diffusion coefficient of the scalar. In the simulations, the scalar diffusivity in terms of the Schmidt number is $\mathrm{Sc}=\nu/\mathcal{D}=1$.

III. NUMERICAL METHOD

Spatial integration of the governing equations is achieved by employing a formally sixth-order compact finite-difference scheme for the derivatives.[22] In the nonperiodic directions, schemes of reduced order are used at the two nodes adjacent to the boundary. At the node directly on the boundary, a one-sided third-order scheme is applied, and at the consecutive node a central fourth-order scheme is used. For the temporal integration, an explicit four-stage Runge-Kutta scheme of third order[23] is employed.

The computational domain is a rectangular box with a domain size, in terms of the jet inlet height h, of $L_x/h=47$,

$L_y/h=18$, and $L_z/h=9.6$ in the streamwise, wall-normal, and spanwise directions, respectively. In the simulation, the streamwise and the wall-normal directions are nonperiodic, while in the spanwise direction periodic boundary conditions are used. The number of nodes used in the simulation is $384\times192\times128$, in the streamwise, wall-normal, and spanwise direction, respectively. The smallest scales present in the wall-jet are found in the near-wall region, in analogy to other wall bounded flows. This can be concluded by observing that the dissipation maximum occurs at the wall, see Fig. 16. Wall units are consequently used to quantify the resolution. In the streamwise direction, a third-order polynomial is used to stretch the grid. The grid spacing is finest in the transition region of the jet, and coarsest at the outlet, maintaining a node separation of $10<\Delta x^+<11$ in terms of wall units in the region used for turbulence statistics $15\leqslant x/h\leqslant40$. The spanwise node separation, also in wall units, decreases from $\Delta z^+(x/h=15)=8.2$ to $\Delta z^+(x/h=40)=5.5$ in the same region. The resolution in these directions is comparable to the resolution in channel flow simulations.[24] In the wall-normal direction, the grid is stretched using a combination of a hyperbolic tangent and a logarithmic function. The combination allows for clustering of nodes close to the wall while maintaining a high resolution of the outer layer. In the inner region, the viscous sublayer ($y^+<5$) is always resolved with three or more nodes. In the outer layer, the wall-normal node spacing equals that of the spanwise direction at a wall distance $y/h=2.9$.

To avoid accumulation and growth of unresolved waves in the high wave number range, a low-pass filter is continuously applied to the scalar and velocity fields. Filtering of the fluid variables is performed once every ten time steps using the explicit sixth-order filter suggested by Lele.[22] In an effort to prevent negative concentrations, owing to dispersion errors of the numerical scheme, a second-order filter is applied to the scalar concentration in the initial part of the domain, $x/h<12$. The inlet region is filtered with a longer interval, once every 300 time steps, to reduce the introduced numerical diffusivity. In the rest of the domain, the scalar is filtered using the same filter and the filtering period as the fluid variables. This approach did reduce but not completely prevent negative scalar concentration. The second-order filter completely avoids the creation of negative concentration in the initial region. Further downstream, spots of negative concentration appear in the far outer part of the jet. The magnitude of these is in general less than 4% of the inlet scalar concentration.

To validate that the results are independent of the grid resolution and domain size, a reference simulation was carried out. In the reference simulation, a domain size of $25h\times15h\times4.8h$ consisting of $160\times160\times50$ nodes was used. The smaller simulation yielded results very close to the ones presented in the article concerning jet growth, mean velocity profiles, and Reynolds shear stress.

IV. INLET AND BOUNDARY CONDITIONS

The inlet profiles for the velocity and the scalar concentration are shown in Fig. 1 and are described in detail in Appendix A 1. The velocity profile includes a coflow of 10% of the jet inlet velocity, $U_c=0.10U_{\text{in}}$. The purpose of the coflow is to ensure that large-scale vortices, propagating out from the jet, leave the domain without contaminating the statistics. The inlet scalar profile is finite at the wall, assuming that the scalar is homogeneously mixed in the injected fluid prior to injection. At the wall, a no-flux condition, $(\partial\theta/\partial y)_{y=0}=0$, is applied. The scalar is initially zero in the coflow above the jet.

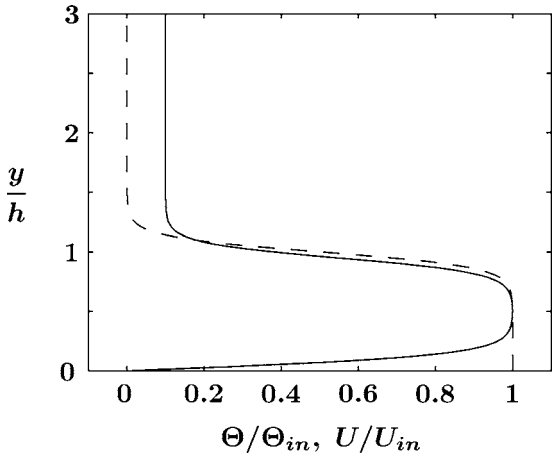

FIG. 1. Inlet profiles for the velocity (solid) and scalar concentration (dashed).

We define the velocity half-width $y_{1/2}$ as the distance from the wall to the position with a mean velocity of half of the excess value, $U(y_{1/2})=\frac{1}{2}(U_m-U_c)$, and the corresponding scalar half-width $y_{1/2}^{\theta}$ as the distance to the position with half of the maximum concentration, $\Theta(y_{1/2}^{\theta})=\frac{1}{2}\Theta_m$. At the inlet, $y_{1/2}=y_{1/2}^{\theta}=h$. The Reynolds number based on the inlet height is $\text{Re}=U_{\text{in}}h/\nu=2000$, and the inlet Mach number used is $M=U_{\text{in}}/a=0.5$, where a is the speed of sound.

Inlet disturbances are introduced to facilitate a fast transition to turbulence, so that in a large part of the domain the flow is fully turbulent. Three types of disturbances are used in the present simulation: random disturbances of a prescribed length scale, streamwise vortices, and periodic streamwise forcing. All disturbances are superimposed at the inlet. The random disturbances are generated using a digital filter technique by Klein *et al.*[25] The filter produces correlated disturbances with a length scale of $h/3$ and a root-mean-square magnitude of $0.05U_{\text{in}}$. Streamwise vortices are added in the upper shear layer. This disturbance type was found by Levin *et al.*[19] to play an important role in plane-jet transition. The amplitude of the added vortices is $0.01U_{\text{in}}$. The streamwise periodic disturbance is composed of two harmonic functions, each with an amplitude of $5\times10^{-3}U_{\text{in}}$ and a respective Strouhal number of 0.3 and 0.45. The inlet disturbances are defined in more detail in Appendix A 2. At the top of the domain, an inflow velocity is applied to account for the entrainment of fluid caused by the jet. The top inflow condition used is defined in Appendix A 3.

To minimize the reflection and generation of spurious waves at the boundaries, boundary zones in the manner of Freund[26] are used. The zones consist of two additional terms,

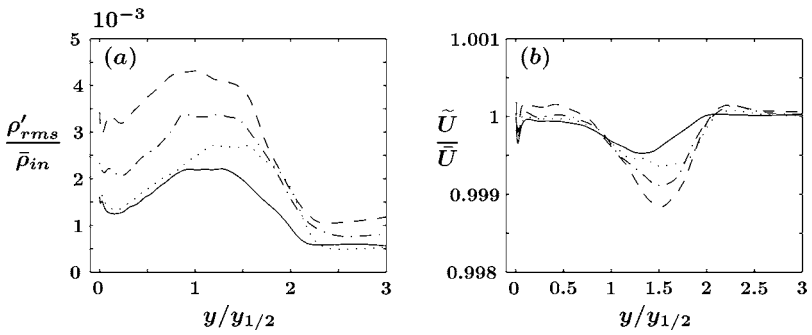

FIG. 2. Density fluctuation intensity (a) and the ratio of the Favre and Reynolds averaged mean streamwise velocity (b). Profiles at downstream positions of $x/h=15$ (dashed), $x/h=20$ (dashed-dotted), $x/h=30$ (dotted), and $x/h=40$ (solid).

one convective and one dissipative, added smoothly to the equations in the vicinity of the inlet, outlet, and the top boundary. The thickness of the boundary zones is approximately h at the inlet, $2.5h$ at the outlet, and $4h$ at the top. A more complete description of the boundary zones is available in Ahlman *et al.*[27]

V. RESULTS

To accumulate statistics, the solution was sampled every 200 time steps corresponding to approximately $0.5t_j$, where $t_j=h/U_{\text{in}}$ is the inlet time scale. The sampling was started at $t=185t_j$ and continued for a duration of $t_{\text{samp}}=309t_j$. Because of the slow time scales in the end of the domain, such a long simulation time is required to obtain reliable statistics. The simulation was performed on a Linux cluster using 22000 CPU hours.

To account for compressibility, statistics is commonly computed using mass-weighted (Favre) averaging. Assuming a variable f, the decomposition into a mean and fluctuating part is performed through

$$f=\tilde{f}+f''=\overline{\rho f}/\bar{\rho}+f'', \tag{6}$$

where ρ is the fluid density and the usual averaging procedure is denoted by $\bar{f}$. The mass-weighted mean is denoted by $\tilde{f}$ and the corresponding fluctuation by f''. In the simulation results, Favre averaged statistics are denoted by plain uppercase letters, e.g., $U=\tilde{U}$.

In Fig. 2, the density fluctuation intensity normalized by the inlet density and the ratio of the Favre and Reynolds averaged streamwise velocity are presented. The density fluctuations and their effect on the averaged statistics are small $[\mathcal{O}(10^{-3})]$ and decrease downstream. Compressibility effects are thus small and can in fact be neglected in the present analysis. Nevertheless, Favre averaging has been used to compute the statistics presented.

Figure 3 shows a snapshot of the streamwise velocity and the scalar concentration in an xy plane. The transition process can be seen to start prior to $x/h=5$, after which the flow quickly becomes fully turbulent. Instantaneous plots of the scalar fluctuation, θ''/Θ_m, in two downstream cross-flow planes (zy planes) at $x/h=20$ and 40 are shown in Fig. 4, where it can be noted that the scales of the flow structures grow significantly downstream, in particular in the outer part of the jet.

In Fig. 5, an instantaneous plot of the streamwise velocity fluctuation u''/u_τ is shown in an xz plane close to the wall at $y^+=9$. In this region, elongated streamwise streaks, typical of boundary layers, are present.

A. Jet development

In the next section, we investigate the velocity statistics in the inner and outer shear layers, using appropriate inner and outer scaling techniques. This approach alleviates comparisons with other results at higher Reynolds numbers. The downstream development of friction velocity, $u_\tau=\sqrt{\tau_w/\rho}$, and wall scalar concentration, Θ_w, both normalized by inlet values, are presented in Fig. 6. The friction velocity exhibits an initial decrease due to laminar propagation. Further down-

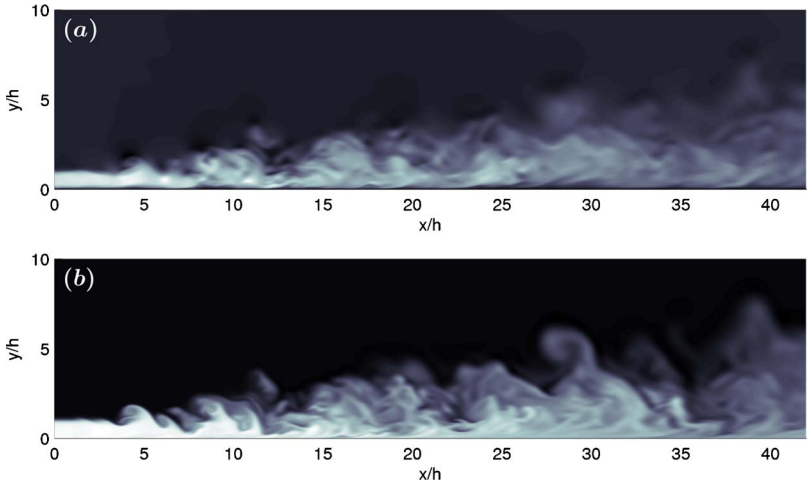

FIG. 3. Instantaneous plots of the streamwise velocity (a) and the scalar concentration (b) in an xy plane. For the velocity, a light color corresponds to a high velocity and dark to a low velocity (or locally negative). For the scalar, a light color corresponds to a high concentration and dark represent zero concentration.

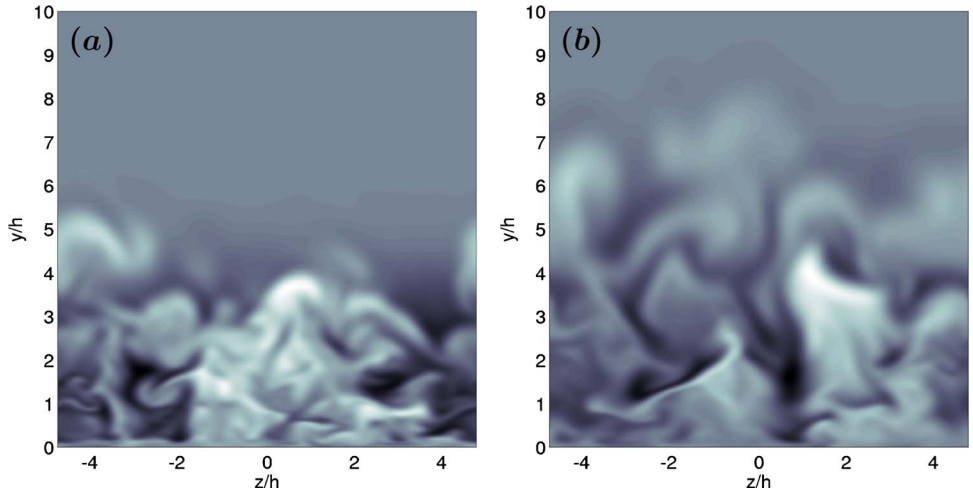

FIG. 4. Instantaneous plots of the scalar fluctuation θ''/Θ_m in two cross stream planes (zy planes) at $x/h=20$ (a) and at $x/h=40$ (b). A light color corresponds to a positive fluctuation and dark a negative.

stream, in the transition region, the friction velocity increases, until approximately $x/h=11$, whereafter turbulent propagation causes a monotonic decrease. The small wiggle noted near $x=0$, an artefact of the boundary technique, occurs solely in the sponge zone and does not affect the flow in the interior domain. The wall scalar concentration remains virtually constant prior to the transition start, exhibits a slight decrease during transition, and a substantial decrease beyond $x/h=11$.

The downstream development of the velocity and scalar half-widths in the simulation as well as the velocity half-width from the experiments by Eriksson *et al.*[9] are plotted in Fig. 7. The velocity half-width growth in the initial region is seen to be different in the simulation and the experiments. In particular, the transition to turbulence in the simulation appears to be faster. This is a result of the efficient, high-amplitude inlet disturbances used. In the experiment, natural, low-magnitude turbulent disturbances, or remnants thereof, are present at the inlet and therefore the transition is more gradual. As a consequence of the different transition scenarios, the virtual origins of the simulation and experimental half-widths differ. In both the DNS and the experiment, the developed turbulent growth of $y_{1/2}$ is approximately linear, in correspondence to what is found in self-similar plane free jets. Fitting a linear relation, using values from $x/h=15$ to 40, yields a half-width growth rate of $dy_{1/2}/dx=0.068$ in the simulation. This is somewhat lower than the range $dy_{1/2}/dx=0.073\pm0.002$ deduced by Launder and Rodi,[5] and the growth rate $dy_{1/2}/dx=0.078$ by Eriksson *et al.*[9] It is also lower than the growth rate $dy_{1/2}/dx=0.081$ reported by Abrahamsson *et al.*[7] This lack of universality is well known from previous wall-jet studies[4,7,11,13] and can be attributed to the differences in Reynolds number[7,11] and the use of a coflow in the simulation.[13] The growth rate of the scalar half-width is approximately equal to that of the velocity. This is in contrast to the corresponding property in plane jets, where the downstream scalar growth rate has been reported to be greater than the velocity-based one.[28–30]

In Fig. 8, the streamwise decay ratio $(U_{\text{in}}-U_c)^2/(U_m-U_c)^2$ is plotted as a function of x/h. In the turbulent part, this quantity appears to be linear, in correspondence to the decay of a plane jet, for which self-similarity analysis yields $U_m\sim 1/\sqrt{x}$.[31] The fast transition in the simulation is again evident. The streamwise decay ratio adjusts to an approximately linear relation already at $x/h=15$, whereas in the experiments this happens further downstream. After $x/h=70$, the linear growth rate is close to that of the simulation, suggesting that the experiments become self-similar significantly further downstream than the simulation.

B. Velocity field statistics

In Fig. 9, mean streamwise velocity profiles are plotted in inner scaling using the friction velocity $u_\tau=\sqrt{\tau_w/\rho}$ and the viscous length $l_*=\nu/u_\tau$ as characteristic inner scales, in correspondence to boundary layers. The inner scaling is found to collapse the near-wall portion of the wall-jet mean profiles. In order to compare the inner region with that of a boundary layer, the simulation data of Skote *et al.*[32] at $\text{Re}_{\delta^*}=200$ are added in the figure. Our data and the boundary layer data are seen to agree well, in terms of the inner scaling, to $y^+=13$. An inertial sublayer is presumed to exist far-

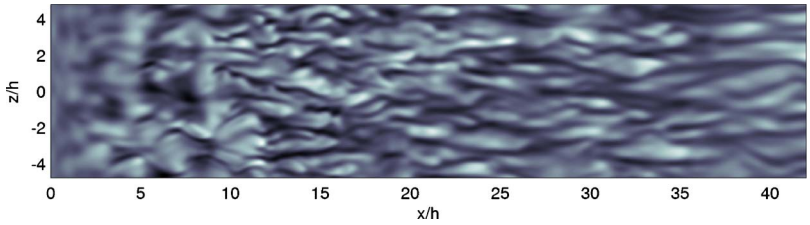

FIG. 5. Instantaneous plot of the velocity fluctuation u''/u_τ in an xz plane at $y^+=9$. A light color corresponds to a positive fluctuation and dark a negative.

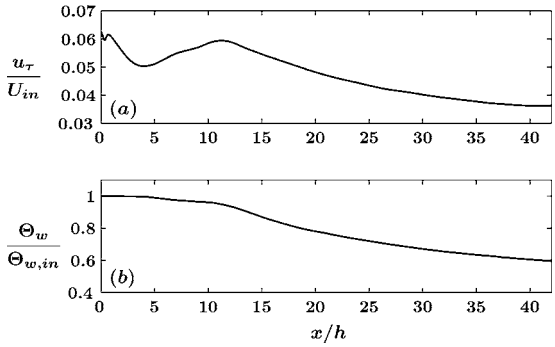

FIG. 6. Downstream development of the friction velocity u_τ/U_{in} (a) and the wall scalar concentration $\Theta_w/\Theta_{w,\text{in}}$ (b).

ther out from the wall, provided that the Reynolds number is high enough. Logarithmic overlap regions have been found in previous wall-jet investigations by Wygnanski *et al.*,[11] Eriksson *et al.*,[9] and Dejoan and Leschziner,[15] but no logarithmic region is found in the profiles extracted from the DNS. Evidently the low Reynolds number, Re=2000, does not allow for large enough scale separation.

Since the inner scaling does not apply outside of $y^+=13$, another scaling is applied to the center region of the jet in Fig. 10. The wall distance is scaled with the half-width $y_{1/2}$ and the velocity with the local maximum velocity U_m. This corresponds to the conventional outer scaling and has previously been used to collapse profiles in wall-jets without coflow.[5,7–9] In this scaling, the profiles collapse in the inner shear layer and in the center region of the jet. However, very close to the wall the inner scaling applies, as shown before. At all downstream positions, the maximum streamwise velocity is found at $y_m/y_{1/2}\approx 0.24$, which is higher than the value 0.17 quoted by Eriksson *et al.*[9] and the range 0.13–0.17 by Launder and Rodi,[5] but these values were acquired at higher Reynolds numbers and in wall-jets without external streams. Zhou and Wygnanski[13] observed that the ratio $y_m/y_{1/2}$ increases with the inlet coflow ratio U_c/U_{in}. Because of the constant coflow, the conventional outer scaling fails to collapse the mean profiles far out from the wall, especially for $y/y_{1/2}>1$, as seen in 10.

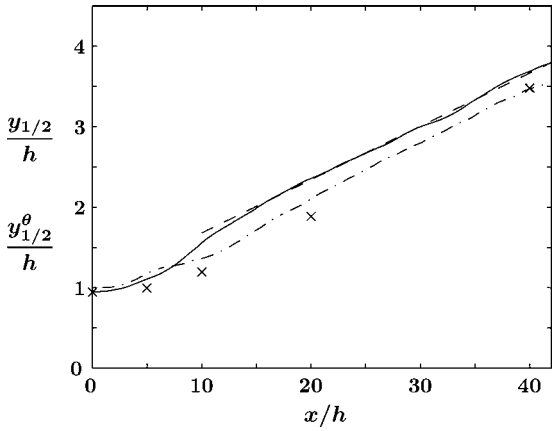

FIG. 7. Wall-jet growth rate; velocity half-width $y_{1/2}/h$ (solid), linear fit (dashed), scalar half-width $y^\theta_{1/2}$ (dash-dotted), and experimental values for the velocity half-width by Eriksson *et al.* (Ref. 9) (×).

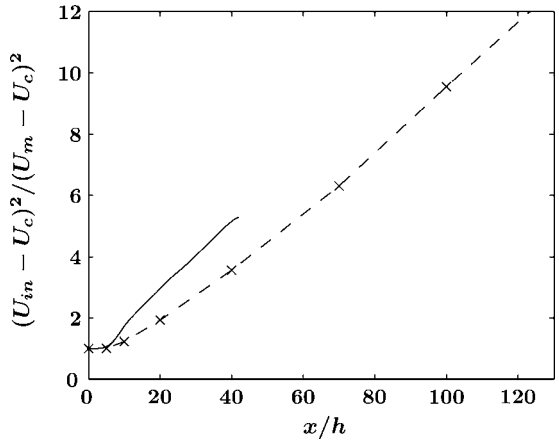

FIG. 8. Decay of streamwise mean velocity against downstream distance. Simulation (solid) and experimental data by Eriksson *et al.* (Ref. 9) (-×-).

Figure 11 shows the streamwise velocity profiles in the outer layer, using an outer scaling adjusted for the coflow. The wall distance is scaled by $y_{1/2}$ and the velocity difference $(U-U_c)$ is scaled by the excess velocity of the outer layer (U_m-U_c). This scaling was suggested by Zhou and Wygnanski[13] for wall-jets with a coflow and yields a good collapse of the velocity profiles in the outer region. Irwin[12] used a classical momentum balance analysis to show that to admit exact self-similarity, the velocity excess to coflow ratio $(U_m-U_c)/U_c$ must be kept constant. The collapse of the mean profiles in the outer layer, therefore, indicates that the constant coflow in the simulation only causes a slight departure from self-similarity.

The fluctuation intensities (root-mean-square profiles) and the turbulent kinetic energy in inner scaling are shown in Fig. 12. The impact of the wall on the wall-normal fluctuations is clearly seen since this component does not have a peak in the inner shear layer. Close to the wall, the wall-normal fluctuations are significantly smaller than the other components, leading to a strong anisotropy. The profile of

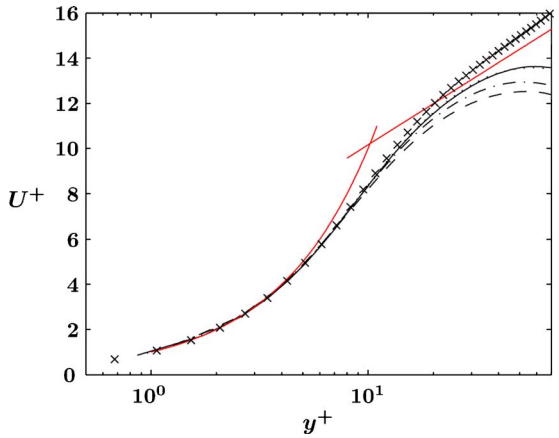

FIG. 9. Mean velocity profiles in inner scaling ($U^+=U/u_\tau$, $y^+=yu_\tau/\nu$) at different downstream positions; $x/h=15$ (dashed), $x/h=20$ (dashed-dotted), $x/h=30$ (dotted), and $x/h=40$ (solid). The linear viscous relation $U^+=y^+$, the logarithmic inertial relation $U^+=\frac{1}{0.38}\ln(y^+)+4.1$ from Österlund (Ref. 33), and DNS data at $\text{Re}_{\delta^*}=200$ from Skote *et al.* (Ref. 32) (×) are also shown.

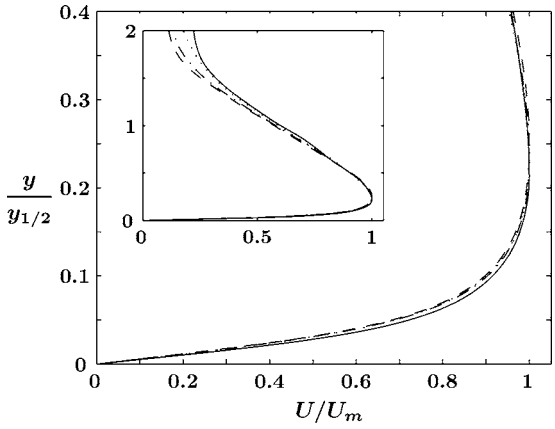

FIG. 10. Mean velocity profiles using conventional outer scaling. Inset shows the full profiles using the same scaling. Lines as in Fig. 9.

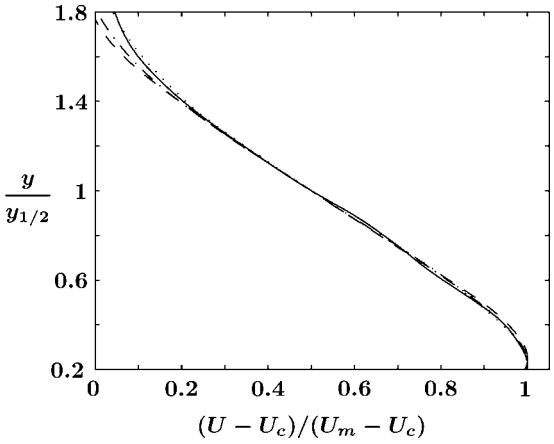

FIG. 11. Mean velocity profiles in the outer shear layer, using an outer scaling adjusted for the coflow. Lines as in Fig. 9.

the streamwise component has two peaks, in the inner and outer layers, respectively. The inner peak is positioned at $y^+=13$, which is in agreement with zero pressure gradient boundary layer data.[33] The inner maximum streamwise fluctuation intensity is approximately $u^+=2.4$, which is in reasonable agreement with Spalart,[34] who found a value of $u^+=2.51$ in a boundary layer at $\mathrm{Re}_\theta=300$, and Moser *et al.*,[35] who reported a value of $u^+=2.66$ in a channel flow at $\mathrm{Re}_\theta=180$. The maximum production of kinetic energy in the inner layer (not shown here) is found to be positioned at $y^+=10$. In between the inner and outer layer u^+ maxima, the fluctuation intensity minimum is positioned at $y^+=50$, corresponding to the U_m position (see Fig. 9) where production due to mean shear vanishes. Both streamwise fluctuation peaks are of the same magnitude in contrast to experiments performed at higher Reynolds numbers,[7,9] where u^+ is higher in the outer region.

The spanwise velocity fluctuation profile does not show a peak near the wall, but rather a plateau. In the outer part, the w^+ profiles are similar to those of the other components. Regarding scaling in the inner part, $y^+<13$, both the u^+ and v^+ profiles collapse well. This is expected from the collapse of the mean profiles and the good agreement with boundary layer data in this region in terms of inner scaling. Comparing the intensity profiles in the outer shear layer, they all appear to collapse using inner scaling and to have peaks positioned close to $y^+=200$.

The experimental streamwise and wall-normal fluctuation intensity profiles of Eriksson *et al.*[9] at $x/h=70$ are also plotted in inner scaling in Fig. 12. This downstream station is used to ensure a comparison in the respective self-similar regions of the simulated and the experimental wall-jets. The wall-normal intensity in the inner layer compares well with the experimental values. In the streamwise component, however, the fluctuation intensity is significantly lower in the simulation. This difference is, at least partly, a Reynolds number effect.

The turbulent fluctuation intensities and the turbulent kinetic energy are evaluated using an outer scaling in Fig. 13.

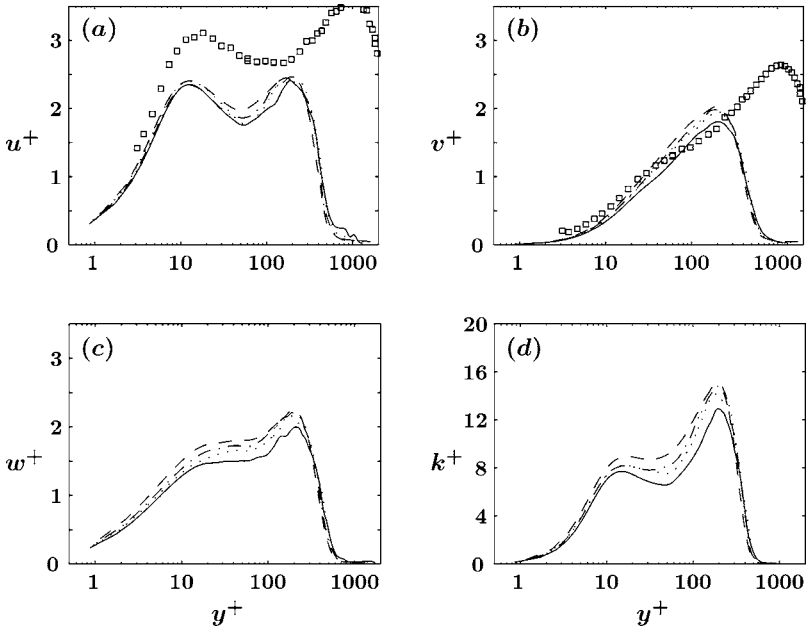

FIG. 12. Individual velocity fluctuation intensities (a)–(c), and the turbulent kinetic energy (d) using inner scaling ($u^+=u''_{\mathrm{rms}}/u_\tau$, $k^+=k/\frac{1}{2}\bar{\rho}u_\tau^2$). Simulation profiles at downstream positions of $x/h=20$ (dashed), $x/h=25$ (dashed-dotted), $x/h=30$ (dotted), and $x/h=40$ (solid). Experimental profiles (Ref. 9) at $x/h=70$ (□).

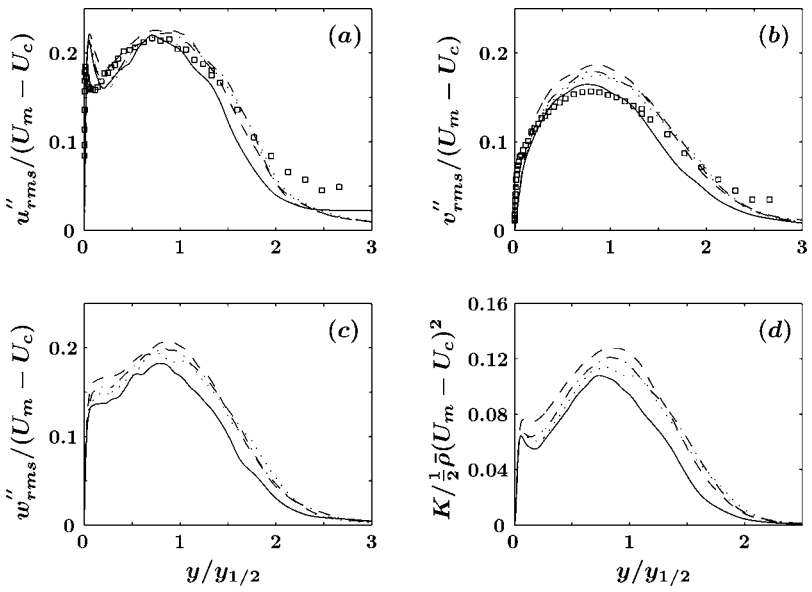

FIG. 13. Streamwise $[u''_{\mathrm{rms}}/(U_m-U_c)]$, wall-normal $[v''_{\mathrm{rms}}/(U_m-U_c)]$, and spanwise $[w''_{\mathrm{rms}}/(U_m-U_c)]$ velocity fluctuations (a)–(c), and the turbulent kinetic energy $\left[K/\frac{1}{2}\bar{\rho}(U_m-U_c)^2\right]$ (d), using outer scaling. Lines as in Fig. 12. Experimental profiles (Ref. 9) at $x/h=70$ (□).

The outer scaling is based on the excess velocity (U_m-U_c) and the velocity half-width $y_{1/2}$, in analogy to the self-similar scaling of a free shear layer. The outer part of the downstream profiles is found to collapse fairly well in this scaling. The profiles furthermore agree well with the scaled experimental profiles,[9] except for far out from the wall, which can be explained by the difference in ambient flow conditions. The outer fluctuation peaks are positioned approximately at $y=0.8y_{1/2}$, in the vicinity of the mean velocity gradient maximum. In agreement with other typical turbulent shear flows, the streamwise component is larger than the other two components. The scaled maximum streamwise intensity $u''_{\mathrm{rms}}/(U_m-U_c)$ is about 0.22, which is close to the range 0.24–0.3 observed in the self-similar region of plane jets.[29,30,36,37] The maximum of the outer scaled v''_{rms} and w''_{rms} profiles decreases slightly downstream and attains values between 0.17–0.19 and 0.18–0.21, respectively. This is in good agreement with Gutmark and Wygnanski,[36] who found values of 0.19 and 0.20 for the corresponding components in a plane jet. Hence, we conclude that the turbulence in the outer layer of the plane wall-jet closely resembles that of a plane jet.

In Fig. 14, the normalized turbulence intensity u''_{rms}/U, where U is the local mean velocity, is plotted as a function of y^+. This quantity has previously been shown to be constant in the viscous sublayer, taking a value of about 0.4 in both turbulent boundary layers and channel flows.[38] The wall-jet intensity profiles approach values in the range of 0.35–0.39 in the viscous sublayer, which agrees well with the data of Skote *et al.*[32] also presented in the figure.

The Reynolds shear stress is shown in Fig. 15, using inner and outer scaling. Symbols are added marking the U_m and $y_{1/2}$ positions. Experimental profiles[9] are also added for comparison. The inner negative stress peaks at different downstream positions collapse using inner scaling and have a minimum of $uv^+=-0.56$ at $y^+=18$. When increasing the Reynolds number in a channel flow, the inner scaled shear stress peak is found to tend to −1 and to move further out from the wall.[33] This trend is also seen in the wall-jet when comparing the inner layer shear stress to that in the experiments. The outer shear stress maxima are positioned approximately at $0.8y_{1/2}$, similar to the fluctuation intensities in Fig. 13. The outer region shear stress in the simulation is noted to be higher than in the experiment. In the experimental data we have observed that the shear stress increases downstream, indicating a deviation from self-similarity.

The position of vanishing Reynolds shear stress does not coincide with the U_m position. This is a well known property of wall-jets and is evidence of the outer layer interaction with the inner layer. In the simulation, the Reynolds stress vanishes in the range of $43\leqslant y^+\leqslant 49$ for the downstream distance profiles plotted in the figure, while U_m is positioned in the range of $51\leqslant y^+\leqslant 59$. Since the shear stress production term $-\widetilde{u''v''}\partial\tilde{U}/\partial y$ is dominant, this implies that there is a small region where the production of kinetic energy is negative. The production magnitude in this region is, however, not significant. At this Reynolds number the negative production is about two orders of magnitude lower than the maximum production.

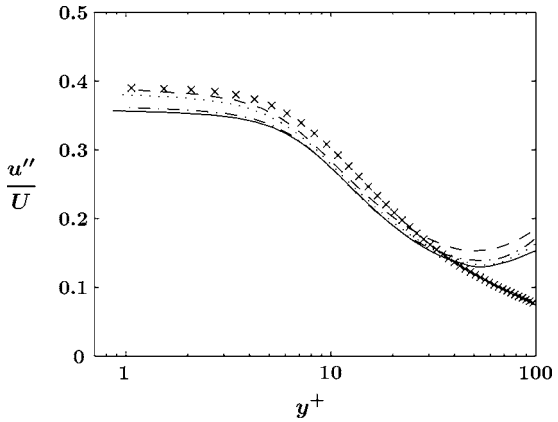

FIG. 14. Near-wall behavior of the local turbulence intensity u''_{rms}/U. Boundary layer simulation by Skote *et al.* (Ref. 32) $\mathrm{Re}_{\delta^*}=200$ (×). Lines as in Fig. 12.

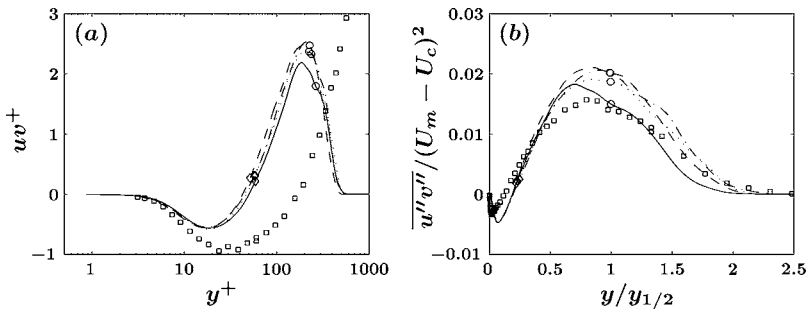

FIG. 15. Reynolds shear stress using inner (a) and outer scaling (b). Symbols mark the U_m ($\diamond$) and $y_{1/2}$ ($\bigcirc$) positions. Lines as in Fig. 12. Experimental profiles (Ref. 9) at $x/h=70$ ($\square$).

George *et al.*[14] proposed that the Reynolds stress should scale with the friction velocity squared, u_τ^2, also in the outer layer. The present data do not clearly support this proposition, because using inner scaling instead of outer does not lead to a better collapse of the profiles.

The viscous dissipation rate, $\epsilon=\tau_{ij}\partial u_i''/\partial x_j/\bar{\rho}$, is presented in Fig. 16. Inner scaling is employed by using u_τ^4/ν, and correspondingly $(U_m-U_c)^3/y_{1/2}$ is used for outer scaling. The near-wall values of ϵ in terms of wall units agree reasonably well with values found in turbulent channel flow. The kink in the profiles at about $y^+=10$ is also present in channel flows.[39] In the outer shear layer, maxima are observed slightly inside of the half-width, coinciding with the position of the Reynolds stress maxima.

C. Scalar statistics

The mean scalar concentration is plotted in Fig. 17 using the scalar half-width $y_{1/2}^\theta$ to scale the wall distance. The concentration profiles are scaled by the maximum concentration Θ_m. The employed scaling leads to a good collapse of the profiles, except for the $x/h=40$ profile in the outer part of the jet, where presumably more samples are required for better statistics.

Profiles of the scalar fluctuation intensity θ_{rms}'' are plotted in Fig. 18 in terms of wall units and the scalar half-width $y_{1/2}^\theta$. From the zero gradient boundary condition on the wall, an inner scaling similar the scaling of the velocity cannot be devised. The local maximum concentration Θ_m is therefore used both as inner and outer scaling for the intensity.

In the near-wall region, the scalar fluctuation is constant, which also is an effect of the scalar boundary condition, and the fluctuation scaling is seen to fail. Outside of the wall region, the fluctuation intensity increases and a maximum intensity is reached near $y=y_{1/2}^\theta$. In the outer region, the intensity scales fairly well with the maximum concentration and the scalar half-width. The scaled maximum intensity is found to be approximately constant, $\theta_{\mathrm{rms}}''\approx 0.18\Theta_m$, throughout a significant part of the outer layer and also to be in good agreement with the values reported for a plane jet by Davies *et al.*,[28] $\theta'\approx 0.19\Theta_m$. In a round jet, the corresponding intensity is higher. Panchapakesan and Lumley[40] reported a value of 0.26 and Chevray and Tutu[41] found approximately 0.24.

The streamwise and wall-normal scalar flux profiles are plotted in Fig. 19. Inner and outer scaling is used for the velocity and the wall distance. As for the fluctuation intensity, the scalar maximum Θ_m is used for both inner and outer scaling. The streamwise flux profiles attain negative values close to the wall, and positive values in the outer layer centered at about $y_{1/2}^\theta$. The maximum streamwise flux magnitude is comparable to the maximum wall-normal flux and is about 0.018 in terms of the outer scaling. For a plane jet, Ramparian and Chandrasekhara[29] found the equivalently scaled streamwise and wall-normal fluxes to be 0.024 and 0.018. In a round jet, Panchapakesan and Lumley[40] found the corresponding fluxes to be about 0.031 and 0.021. The nonzero streamwise flux in the simulation implies that the scalar flux vector is not aligned with the mean scalar gradient, which in close approximation is pointing in the wall-normal direction. The origin of this misalignment of the scalar flux vector can be explained by considering the production of scalar flux in a plane shear layer. When neglecting streamwise mean development, the streamwise production is[42]

$$P_{\theta x}=-\overline{uv}\frac{\partial\Theta}{\partial y}-\overline{v\theta}\frac{\partial U}{\partial y}, \tag{7}$$

where the first term represents production due to the mean scalar gradient and the second production due to mean shear. Both production terms are nonzero in the wall-jet and therefore produce a scalar flux also in the streamwise direction.

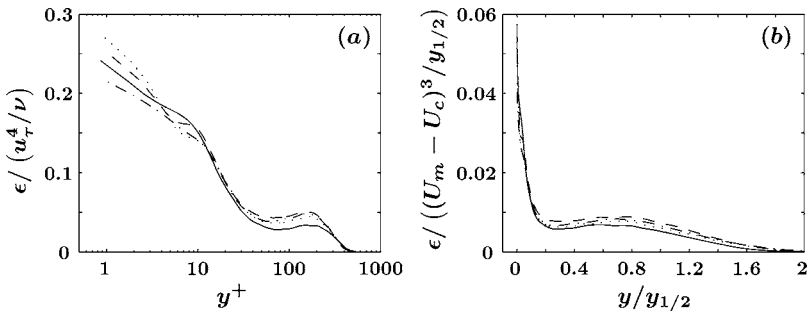

FIG. 16. Viscous dissipation rate using inner (a) and outer scaling (b). Lines as in Fig. 12.

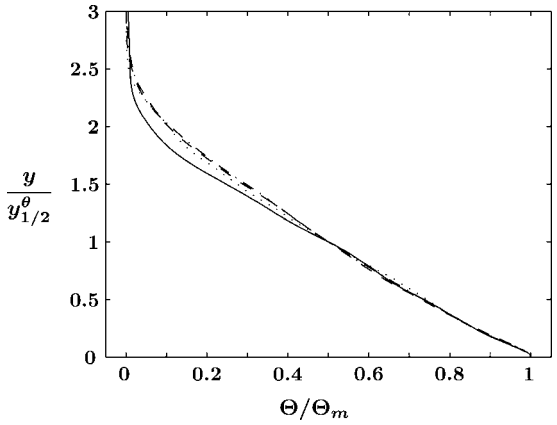

FIG. 17. Mean scalar concentration using outer scaling. Lines as in Fig. 9.

The scalar dissipation rate, $\chi=2\overline{\rho\mathcal{D}\partial\theta''/\partial x_i \partial\theta''/\partial x_i}$, is shown in Fig. 20 scaled with an inlet-based scaling and an appropriate outer scaling. At the first two profile positions, the scalar dissipation possesses a visible inner peak. Further downstream, the scalar dissipation profiles attain a flatter shape, indicating a more homogeneous small-scale mixing throughout the jet. At the same time, the overall dissipation magnitude decreases substantially downstream. As in previous statistics, an appropriate outer scaling approximately collapses the scalar dissipation in the outer layer.

The mechanical to mixing time scale ratio $\tau_\epsilon/\tau_\theta=(K/\epsilon)/(\overline{\theta''^2}/\chi)$ characterizing the small-scale mixing is plotted in Fig. 21. The time scale ratio increases out from the wall and reaches a peak value of about 1.3 at the half-width position. The profiles are qualitatively in agreement with results found in a turbulent channel flow in Johansson and Wikström,[43] where the corresponding time scale ratio was seen to increase in the outer region, reaching a maximum value of about 1.6. The mixing ratio profiles at different downstream positions are also noted to collapse, indicating that the small-scale dynamics and mixing are approximately in equilibrium.

VI. CONCLUSIONS

Direct numerical simulation of a plane compressible wall-jet in a constant coflow, including the mixing of a passive scalar, was performed. The Mach number in the simulation was moderate and compressibility effects were negligible. Statistics from the simulation were computed and analyzed in order to study the wall-jet dynamics and mixing. The statistics were compared to experimental and simulation data of wall-jets and other wall bounded and free shear flows. The growth of the jet was found to be approximately linear with a rate of $dy_{1/2}/dx=0.068$. Also the maximum velocity decay, in terms of $(U_{in}-U_c)^2/(U_m-U_c)^2$, was found to be approximately linear. To investigate self-similarity in the wall-jet inner and outer shear layers, inner and outer scaling was employed. The applied inner scaling corresponds to the boundary layer scaling in terms of plus units. The outer scaling was based on the velocity half-width and the outer excess velocity (U_m-U_c). The study has shown that several statistical quantities have reached an approximate self-similar state in terms of the applied scalings. The use of inner and outer scalings also facilitated comparisons with previous LES and experimental data at higher Reynolds numbers by studying statistics in the inner and outer layers separately.

The inner part of the wall-jet, out to $y^+=13$, was found to closely resemble a turbulent zero pressure gradient boundary layer. In the inner part, the mean and fluctuation profiles collapse in inner scaling and a viscous sublayer is present out to $y^+=5$. The position and magnitude of the maximum streamwise fluctuation intensity agree well with boundary layer data. In the viscous sublayer, the local turbulence intensity tends to be constant in resemblance to boundary layers and channel flows.

The outer layer, on the other hand, resembles a free plane jet. The mean profiles in this region scale with an outer scaling similar to the one used in self-similarity studies of plane jets. The scaled maximum fluctuation magnitudes in the outer shear layer agree well with the wall-jet experiments by Eriksson *et al.*[9] and also reasonably well with data from plane jet experiments.

The downstream growth rate of the scalar in terms of the scalar half-width was found to be approximately equal to the growth rate of the velocity half-width. Scaling with the maximum concentration and the scalar half-width leads to a collapse of the mean scalar profiles. The scalar fluctuation is constant in the viscous sublayer but no appropriate inner scaling exists as a result of the zero-gradient wall boundary condition. The scaled maximum scalar fluctuation in the outer layer corresponds to values observed in free plane jets. The streamwise and wall-normal scalar fluxes were found to be of comparable magnitude, implying that the scalar flux vector and the mean scalar gradient are misaligned. The profiles of the mechanical to mixing time scale at different

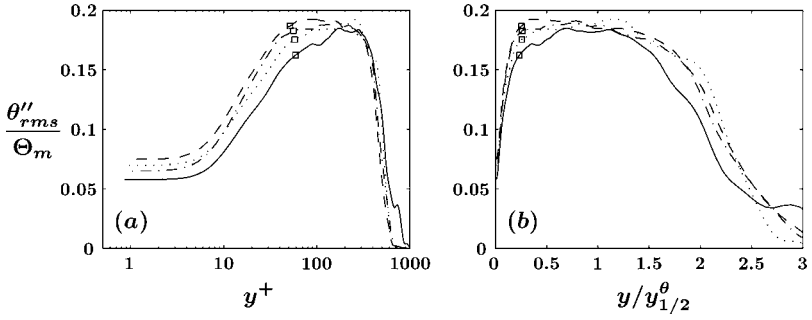

FIG. 18. Scalar fluctuation intensity using inner (a) and outer (b) scaling of the wall distance. Symbols (□) mark the U_m positions. Lines as in Fig. 12.

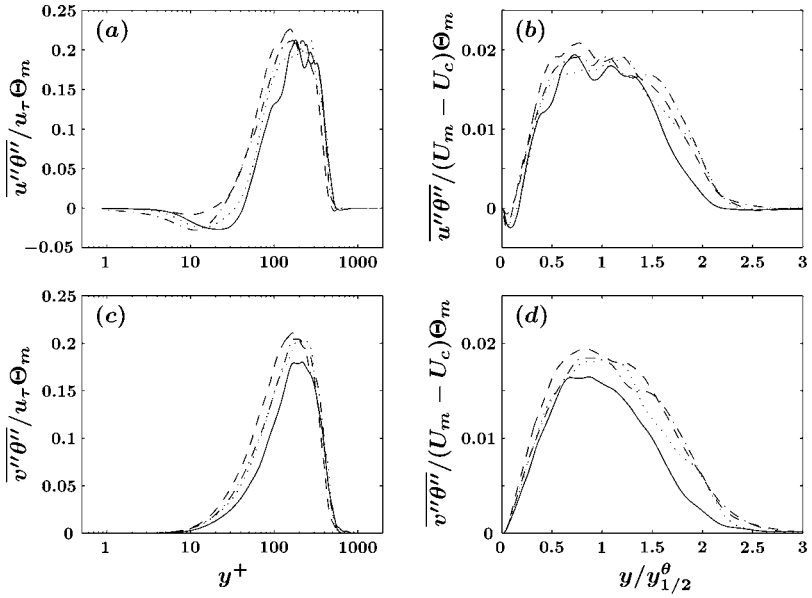

FIG. 19. Streamwise and wall-normal scalar flux using inner [(a) and (c)] and outer [(b) and (d)] scaling. Lines as in Fig. 12.

downstream positions collapse, indicating that the small-scale mixing has reached equilibrium.

ACKNOWLEDGMENTS

The present work has been funded by the Centre for Combustion Science and Technology (CECOST). The computations were performed at the Center for Parallel Computers at KTH, using time granted by the Swedish National Allocation Committee. Professor Bendiks Jan Boersma is thanked for providing the original version of the DNS code. Timmy Sigfrids and Henrik Alfredsson are thanked for discussions on compressibility effects.

APPENDIX: INLET CONDITIONS

1. Inlet profiles

The specified inlet velocity $U_{\text{inlet}}(y)$ consists of a composite profile, constructed from three parts, and is defined as

$$U_{\text{inlet}}(y) = \begin{cases} U_{\text{inner}}(y), & 0 \leqslant y \leqslant y_{c1}, \\ U_{\text{center}}(y), & y_{c1} \leqslant y \leqslant y_{c2}, \\ U_{\text{outer}}(y), & y_{c2} \leqslant y \leqslant L_y, \end{cases} \tag{A1}$$

with connecting points $y_{c1}=0.46h$ and $y_{c2}=0.54h$. The full profile is constructed to have continuous first derivatives at the connecting points. The individual profile parts are defined as

$$U_{\text{inner}}(y) = U_{\text{in}} \tanh\left[G_i\left(\sqrt{(y-c_i)^2} - \frac{w_i}{2} \right) \right], \tag{A2}$$

$$U_{\text{center}}(y) = -a_c y^2 + b_c y + c_c, \tag{A3}$$

$$U_{\text{outer}}(y) = \frac{U_{\text{in}}}{2}\left(1 + \frac{U_c}{U_{\text{in}}} \right) \times \left\{ 1 - \tanh\left[G_o\left(\sqrt{(y-c_o)^2} - \frac{w_o}{2} \right) \right] \right\}. \tag{A4}$$

using profile coefficients in Table I.

The inlet passive scalar profile is prescribed by a using a hyperbolic tangent function

$$\theta_{\text{inlet}}(y) = \frac{\theta_{\text{in}}}{2}\{1 - \tanh[G_t(\sqrt{y^2} - h)]\}. \tag{A5}$$

2. Inlet disturbances

For fast transition to turbulence, three types of inlet disturbances are used in the simulation: random disturbances with a prescribed length scale, streamwise vortices, and pe-

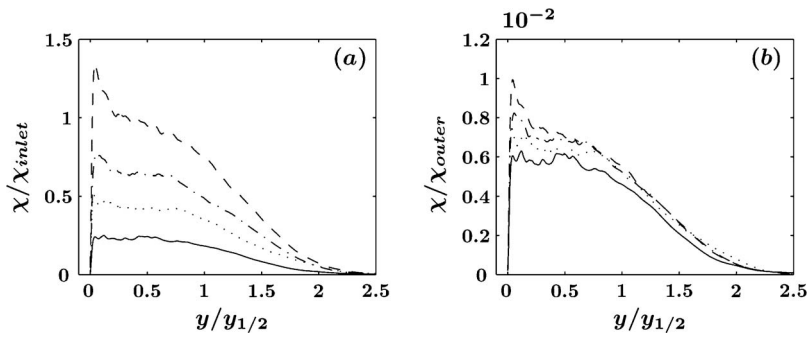

FIG. 20. Scalar dissipation rate using an inlet scaling where $\chi_{\text{inlet}}=2\bar{\rho}_{\text{in}}\mathcal{D}(\Theta_m/h)^2$ (a) and outer scaling where $\chi_{\text{outer}}=\Theta_m^2(U_m-U_c)/y_{1/2}$ (b). Lines as in Fig. 12.

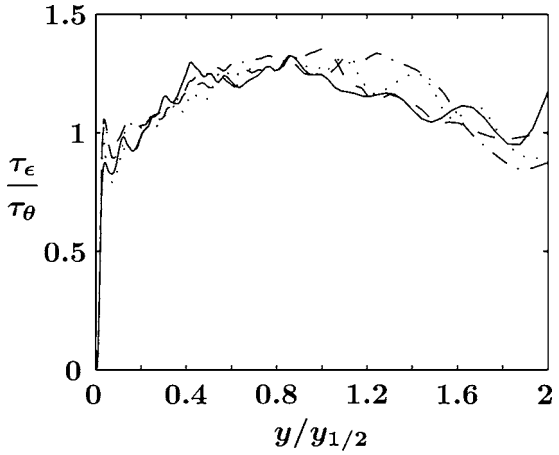

FIG. 21. Time-scale ratio $\tau_\epsilon/\tau_\theta=(K/\epsilon)/(\overline{\theta'^2}/\chi)$. Lines as in Fig. 12.

riodic streamwise forcing. All three disturbances are superimposed at the inlet. The random disturbances are generated using a filter technique by Klein *et al.*[25] The rms magnitude of the random disturbances used is 5% of the jet inlet velocity and the disturbance length scale is $h/3$ in all three directions.

The streamwise vortices are constructed as

$$v_v = A_v \cos\left(\pi\frac{z}{v_w}\right)\sin\left(\pi\frac{y-y_0}{v_w}\right), \tag{A6}$$

$$w_v = -A_v \sin\left(\pi\frac{z}{v_w}\right)\cos\left(\pi\frac{y-y_0}{v_w}\right), \tag{A7}$$

where $A_v=0.01U_{\text{in}}$ is the vortex amplitude, $v_w=0.6h$ is the vortex width, and $y_0=0.6h$ is the lower bound of the vortices.

In the streamwise direction, periodic disturbances of the form

$$u_{\text{st}} = \frac{A_{\text{st}}}{2}\left\{\sin\left[2\pi\text{St}_1\left(\frac{t}{\tau}\right)\right] + \sin\left[2\pi\text{St}_2\left(\frac{t}{\tau}\right)\right]\right\} \tag{A8}$$

are used where $A_{\text{st}}=0.01U_{\text{in}}$ is the disturbance amplitude, $\text{St}_1=0.3$ and $\text{St}_2=0.45$ are the Strouhal numbers employed, and $\tau=h/U_{\text{in}}$ is the characteristic inlet time scale.

3. Top inflow condition

The domain is finite, implying that the entrainment must be accounted for at the top of the domain so that the jet development is not constrained. Carrying out a cross stream integration of the mean two-dimensional continuity equation, an estimation of the mean inflow velocity is found,

$$\frac{\partial\rho U}{\partial x}+\frac{\partial\rho V}{\partial y}=0 \Rightarrow \rho_\infty V_\infty = -\frac{\partial}{\partial x}\int_0^\infty \rho U dy = -\frac{\partial}{\partial x}M_u(x), \tag{A9}$$

where $M_u(x)$ is the streamwise mass flux. Using the data of Eriksson *et al.*,[9] the streamwise mass flux is found to increase linearly according to $M_u(x/h)\sim 0.031M_u^0(x/h)$ in terms of the jet inlet mass flux M_u^0 and the normalized downstream distance. This leads to

$$V_\infty = -0.031M_u^0/h\rho_\infty, \tag{A10}$$

which has been used in the present DNS to prescribe the entrainment velocity at the top of the domain.

TABLE I. Inlet profile coefficients in terms of the jet height $h=y_{1/2}(x=0)=y_{1/2}^\theta(x=0)$.

G_i	c_i	w_i	G_o	c_o	w_o
31.25	0.5	1	31.2789	0.5	0.896917
	a_c		b_c		c_c
	0.589714		0.294857		0.462623

[1] E. Förthmann, "Turbulent jet expansion," NACA TM 789 (English translation) (1936).
[2] M. B. Glauert, "The wall jet," J. Fluid Mech. **1**, 625 (1956).
[3] P. Bradshaw and M. T. Gee, "Turbulent wall-jets with and without external stream," Aeronautics Research Council Reports and Memoranda No. 3252 (1960).
[4] A. Tailland and J. Mathieu, "Jet pariétal," J. Mec. **6**, 103 (1967).
[5] B. E. Launder and W. Rodi, "The turbulent wall jet," Prog. Aerosp. Sci. **19**, 81 (1981).
[6] B. E. Launder and W. Rodi, "The turbulent wall jet—measurements and modelling," Annu. Rev. Fluid Mech. **15**, 429 (1983).
[7] H. Abrahamsson, B. Johansson, and L. Löfdahl, "A turbulent plane two-dimensional wall-jet in a quiescent surrounding," Eur. J. Mech. B/Fluids **13**, 533 (1994).
[8] M. E. Schneider and R. J. Goldstein, "Laser Doppler measurement of turbulence parameters in a two-dimensional plane wall jet," Phys. Fluids **6**, 3116 (1994).
[9] J. G. Eriksson, R. I. Karlsson, and J. Persson, "An experimental study of a two-dimensional plane turbulent wall jet," Exp. Fluids **25**, 50 (1998).
[10] R. Narashima, K. Y. Narayan, and S. P. Parthasarathy, "Parametric analysis of turbulent wall jets in still air," Aeronaut. J. **77**, 335 (1973).
[11] I. Wygnanski, Y. Katz, and E. Horev, "On the applicability of various scaling laws to the turbulent wall jet," J. Fluid Mech. **234**, 669 (1992).
[12] H. P. A. H. Irwin, "Measurements in a self-preserving plane wall jet in a positive pressure gradient," J. Fluid Mech. **61**, 33 (1973).
[13] M. D. Zhou and I. Wygnanski, "Parameters governing the turbulent wall jet in an external stream," AIAA J. **31**, 848 (1993).
[14] W. K. George, H. Abrahamsson, J. Eriksson, R. I. Karlsson, L. Löfdahl, and M. Wosnik, "A similarity theory for the turbulent plane wall jet without external stream," J. Fluid Mech. **425**, 367 (2000).
[15] A. Dejoan and M. A. Leschziner, "Large eddy simulation of a plane turbulent wall jet," Phys. Fluids **17**, 025102 (2005).
[16] M. R. Wernz and H. F. Fasel, "Numerical investigation of unsteady phenomena in wall jets," AIAA Pap. 96–0079 (1996).
[17] M. R. Wernz and H. F. Fasel, "Numerical investigation of forced transitional wall jets," AIAA Pap. 97–2022 (1997).
[18] M. Visbal, D. V. Gaitonde, and S. P. Gogineni, "Direct numerical simulation of a forced transitional plane wall jet," AIAA Pap. 98–2643 (1998).
[19] O. Levin, V. G. Chernoray, L. Löfdahl, and D. S. Henningson. "A study of the Blasius wall jet," J. Fluid Mech. **539**, 313 (2005).
[20] O. Levin, "Numerical studies of transition in wall-bounded flows," Ph.D. thesis, Royal Institute of Technology, Stockholm (2005).
[21] T. Poinsot and D. Veynante, *Theoretical and Numerical Combustion* (R. T. Edwards, Philadelphia, 2001).
[22] S. K. Lele, "Compact finite differences with spectral-like resolution," J. Comput. Phys. **103**, 16 (1992).
[23] A. Lundbladh, S. Berlin, M. Skote, C. Hildings, J. Choi, J. Kim, and D. S. Henningson, "An efficient spectral method for simulation of incompressible flow over a flat plate," Technical report, Department of Mechanics, Royal Institute of Technology (1999).
[24] J. C. del Álamo, J. Jiménez, P. Zandonade, and R. D. Moser, "Self-similar vortex clusters in the turbulent logarithmic region," J. Fluid Mech. **561**, 329 (2006).
[25] M. Klein, A. Sadiki, and J. Janicka, "A digital filter based generation of inflow data for spatially developing direct numerical or large eddy simulations," J. Comput. Phys. **186**, 652 (2003).

[26] J. B. Freund, "Proposed inflow/outflow boundary condition for direct computation of aerodynamic sound," AIAA J. **35**, 740 (1997).
[27] D. Ahlman, G. Brethouwer, and A. V. Johansson, "A numerical method for simulation of turbulence and mixing in a compressible wall-jet," Technical report, Department of Mechanics, Royal Institute of Technology (2006).
[28] A. E. Davies, J. F. Keffer, and W. D. Baines, "Spread of a heated plane turbulent jet," Phys. Fluids **18**, 770 (1975).
[29] B. R. Ramparian and M. S. Chandrasekhara, "LDA measurements in plane turbulent jets," ASME Trans. J. Fluids Eng. **107**, 264 (1985).
[30] S. A. Stanley, S. Sarkar, and J. P. Mellado, "A study of flow-field evolution and mixing in a planar turbulent jet using direct numerical simulation," J. Fluid Mech. **450**, 377 (2002).
[31] S. B. Pope, *Turbulent Flows* (Cambridge University Press, Cambridge, UK, 2000).
[32] M. Skote, J. H. Haritonidis, and D. Henningson, "Varicose instabilities in turbulent boundary layers," Phys. Fluids **14**, 2309 (2002).
[33] J. M. Österlund, "Experimental studies of zero pressure-gradient turbulent boundary layer flow," Ph.D. thesis, Royal Institute of Technology, Stockholm (1999).
[34] P. R. Spalart, "Direct numerical simulation of a turbulent boundary layer up to Re_θ=1410," J. Fluid Mech. **187**, 61 (1988).
[35] R. D. Moser, J. Kim, and N. N. Mansour, "Direct numerical simulation of turbulent channel flow up to Re_τ=590," Phys. Fluids **11**, 943 (1999).
[36] E. Gutmark and I. Wygnanski, "The planar turbulent jet," J. Fluid Mech. **73**, 465 (1976).
[37] F. O. Thomas and K. M. K. Prakash, "An experimental investigation of the natural transition of an untuned planar jet," Phys. Fluids A **3**, 90 (1991).
[38] P. H. Alfredsson, A. V. Johansson, J. H. Haritonidis, and H. Eckelmann, "The fluctuating wall-shear stress and the velocity field in the viscous sublayer," Phys. Fluids **31**, 1026 (1988).
[39] M. Tanahashi, S. J. Kang, T. Miyamoto, S. Shiokawa, and T. Miyauchi, "Scaling law of fine scale eddies in turbulent channel flows up to Re_τ =800," Int. J. Heat Fluid Flow **25**, 331 (2004).
[40] N. R. Panchapakesan and J. L. Lumley, "Turbulence measurements in jets of air and helium. Part 2. Helium jet," J. Fluid Mech. **246**, 225 (1993).
[41] R. Chevray and N. K. Tutu, "Intermittency and preferential transport of heat in a round jet," J. Fluid Mech. **88**, 133 (1978).
[42] P. M. Wikström, S. Wallin, and A. V. Johansson, "Derivation and investigation of a new explicit algebraic model for the passive scalar flux," Phys. Fluids **12**, 688 (2000).
[43] A. V. Johansson and P. M. Wikström, "DNS and modelling of passive scalar transport in turbulent channel flow with a focus on scalar dissipation rate modelling," Flow, Turbul. Combust. **63**, 223 (1999).